Macromolecules
ARTICLE

Macromolecules **2010**, *43*, 837–844 **837**
DOI: 10.1021/ma9019812

Preparation of Polymeric Core−Shell and Multilayer Nanoparticles: Surface-Initiated Polymerization Using *in Situ* Synthesized Photoiniferters

A. M. Imroz Ali and Andrew G. Mayes*

Wolfson Materials and Catalysis Centre, School of Chemistry, University of East Anglia, Norwich NR4 7TJ, U.K.

Received September 4, 2009; Revised Manuscript Received November 26, 2009

ABSTRACT: We report here the development of a very flexible synthetic approach to generate core−shell nanoparticles below 100 nm diameter, whereby thin polymer shells are synthesized under nonaqueous conditions in a variety of organic solvents with diverse properties. This facilitates incorporation of a wide range of functional monomers and cross-linkers in the shell, without the need to make major changes to conditions or methodology. Polymer cores carrying benzyl chloride functionalities were prepared by conventional emulsion polymerization and then derivatized with sodium diethyldithiocarbamate to generate surface bound iniferters. Photoinduced second-stage surface-initiated polymerization (SIP) led to shell formation (measured as an increase in particle size by dynamic light scattering) with good control over the size distribution. The core−shell morphology of the particles generated was confirmed by transmission electron microscope (TEM) imaging and the composition of the shell layer with IR spectroscopy. The presence of ionic functionalities in the shell layer was verified by aqueous zeta potential titration studies. By exploiting the surface-initiated living radical mechanism, we have also synthesized complex multilayer particles sequentially. Even after the formation of an additional layer, the majority of the iniferter groups were re-formed as determined by elemental analysis; therefore, further particle elaboration would be possible if required.

Introduction

During the past decade, discussion of structures and objects with characteristic dimensions between 1 and 100 nm, the nanocosm,[1] has become the focus of intense interest and activity, not only for scientists but also for a broader public. Polymer colloids and particularly latex particles belong to the class of naturally occurring colloidal systems and moreover are one of the oldest synthetically produced and commercially successful applications of polymeric materials. With growing specificity of polymer applications, development of synthetic control is required for the preparation of new polymeric materials with particular physical, chemical, and functional properties. Furthermore, manipulation of polymer architecture and morphology is essential in the design of specific polymeric materials.

Recent challenges and successes of nanoscale science and technology are connected to the production of functional materials and devices in which the individual units and their spatial arrangement are engineered down to the nanometer scale. One promising way of achieving this goal is the production of core−shell composite nanoparticles. Recently, it has become a fast-growing topic in colloid and materials science. Core−shell composite nanoparticles are structured nanoparticles that comprise of a core of one material and a coating shell of another material. They are typically around 20−200 nm in diameter. The utilization of nanoparticles with core−shell or multilayer morphology allows one to obtain complex compositional and structural patterns in the ultimate nanocomposite material. Core−shell composite latex particles are widely used in industrial applications, such as paints, coatings, and adhesives, as they allow combination of the physical properties of two incompatible polymers on small length scales, a task usually difficult to achieve by blending polymers macroscopically.[2,3] Other uses of core−shell structures include drug delivery systems, information storage, pickering emulsifiers, and templating agents as well as many functional composites with inorganic materials. The architecture is particularly interesting because the core can be derivatized to make the particle e.g. fluorescent or magnetic, independent of the shell properties. Such labeled particles have many potential uses in areas such as assay technology, separation science, and imaging. For instance, in assay technology these nanoparticles are of particular interest in developing "antibody mimics" since they can be handled similarly to antibodies. The geometry offers colloidal stability, easy dispensing, high external surface area for analyte adsorption, and (in theory) good binding site accessibility and rapid binding kinetics.

Over the past few decades various techniques have been applied for the preparation of core−shell composite nanoparticles. Generally, a core−shell structure can be achieved by seeded emulsion polymerization,[4−11] seeded dispersion polymerization,[12−17] emulsion polymerization using reactive or polymeric surfactants,[18−20] or heterocoagulation of oppositely charged core and shell particles.[21−28] Furthermore, it is reported that self-assembly of polymer chains on a core surface[29] and layer-by-layer deposition[30−33] are also effective approaches for obtaining core−shell structures. Another alternative method for achieving well-defined core−shell morphology is to graft polymer brushes through the use of initiators tethered chemically to the particle surface.[34−39] This "grafting from" technique offers an opportunity to achieve stable layers of densely grafted polymers with a variety of compositions and functionalities, covalently attached to the surfaces of micro- or nanoparticles.

SIP, in combination with a living or living radical polymerization method, is among the most useful synthetic routes to specifically design and functionalize surfaces with well-defined polymers and copolymers. The implementation of controlled

*To whom correspondence should be addressed. E-mail: andrew.mayes@uea.ac.uk.

Published on Web 12/16/2009

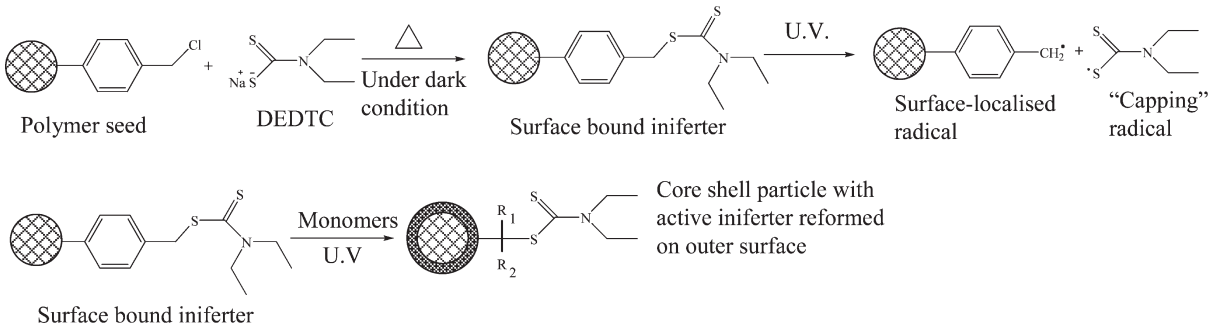

Figure 1. Schematic representation of the surface-bound dithiocarbamate (DTC) iniferter and its subsequent use to graft a shell onto a nanoparticle surface. R_1 and R_2 will vary with the nature of the monomer (e.g., R_1 = H, R_2 = COOH for methacrylic acid).

surface-initiated polymerization to prepare composite nanoparticles is a new and challenging area where fundamental understanding is aiding the development of new functionalities with interesting new applications. SIP has been extensively applied to surface modification of a variety of substrate surfaces[40−49] to produce high-density polymer brushes for diverse applications and has also been used to prepare polymer-coated metal and inorganic nanoparticles.[50−67] Use of this approach to generate core−shell materials with polymeric cores is less common but has been elegantly demonstrated in a number of reports from Kawaguchi's group.[68−70] Polymer cores of 300−400 nm (produced by surfactant-free emulsion polymerization) were coated with long hairy thermoresponsive polymer shells (brushes) using UV-initiated polymerization under aqueous conditions from dithiocarbamate iniferters formed on the particle surface using well-established chemistry originated by Otsu.[71,72] Core−shell structures were also produced using ATRP by Guerrini et al.[73] and by Jayachandran et al.,[74] in a detailed exploration of surface grafting under aqueous conditions.

We have chosen to further explore the iniferter approach due to its high tolerance of monomer functionality and reaction conditions. Our aim is to make polymeric core−shell nanoparticles for use as antibody mimics in a size range comparable with their biological equivalents. We have recently reported preliminary studies on the preparation of molecularly imprinted core−shell nanoparticles by a surface grafting method[75] similar to that used by Kawaguchi. In contrast to Kawaguchi's work, however, our approach has been to develop this "grafting-from" method to generate thin shells on nanosize cores (about 60 nm) under nonaqueous conditions (important for noncovalent molecular imprinting). In this paper we present studies demonstrating the far greater utility and flexibility of this synthetic approach by generating small core−shell nanoparticles with a much wider range of functional monomers and synthetic conditions than those reported in our preliminary work. Using TEM imaging, we confirm for the first time that polymerization indeed leads to a well-defined polymer shell around the original core under our synthesis conditions and that both highly cross-linked and linear polymer shells can be grafted without significant gelation occurring. Finally, it is shown that multilayer structures containing linear polymers or cross-linked networks of different monomers can be grown due to retention of the iniferter by radical recombination at the particle surface.

The strategy uses cores (nanosized seed particles), containing benzyl chloride functionalities, synthesized by conventional emulsion polymerization. The iniferter is formed by reaction of the benzyl chloride groups at the core particle surface with sodium diethyldithiocarbamate (DEDTC).[68] Exposure of the derivatized particle to UV light in the presence of second stage monomers initiates controlled surface-localized polymer growth leading to covalently grafted polymer chains. When the UV is removed, the thiocarbamate radicals recombine with radical chain ends to re-form the active iniferter, which can subsequently be reactivated with other monomers to generate a further shell. A schematic representation of the formation of core−shell nanoparticle is shown in Figure 1.

Experimental Section

Materials. Methyl methacrylate (MMA) (99%) and methacrylic acid (MAA) (99%) from Aldrich were distilled under vacuum to remove inhibitor and stored in a refrigerator, while styrene (St) (99%) from Aldrich was washed with 1 M aqueous sodium hydroxide, dried over magnesium sulfate, and stored with molecular sieves at 4 °C until required. 2-Hydroxyethyl methacrylate (HEMA) (97%) from Alfa Aesar was purified by passing it through a column containing activated neutral aluminum oxide (BDH). *N*-Isopropylacrylamide (NIPAM) (99%), ethylene glycol dimethacrylate (EGDMA) (98%), 2-(diethylamino)ethyl methacrylate (DEAEMA) (98%), divinylbenzene (DVB) (80%), vinylbenzyl chloride (VBCl) (97%), sodium dodecyl sulfate (SDS) (98%), ammonium persulfate (APS) (98%), and sodium diethyldithiocarbamate trihydrate (DEDTC) (reagent grade) were all purchased from Aldrich and used as received. Phophotungstic acid hydrate (PTA) and ruthenium trichloride hydrate from Aldrich were of reagent grade and used as negative and positive staining agents, respectively. Sodium hypochlorite (reagent grade) from Aldrich was used as received. All other chemicals and solvents used were of analytical grade or better. Deionized water was used for the synthesis and purification of the seed latex.

Synthesis of Seed Particles. The polymerization was conducted in a 1 L three-necked jacketed reactor connected to a recirculating water bath to control the temperature. The system was equipped with a condenser, a mechanical overhead stirrer fitted with a Teflon-coated propeller-type stirring paddle, and a gas inlet and outlet to maintain a nitrogen atmosphere inside the reactor. The seed was prepared using a standard batch emulsion polymerization. First, a solution of $NaHCO_3$ (1.0 g, 11.9 mmol) and SDS (1.0 g, 3.5 mmol) in distilled deionized water (495 g) was added to the reactor and purged with nitrogen to remove oxygen under gentle stirring, while increasing the temperature to 75 °C. Once the temperature had reached 75 °C, the monomer mixture (styrene 31.0 g, 297.6 mmol; VBCl 7.8 g, 50.8 mmol; DVB 1.6 g, 11.9 mmol) was introduced into the reactor and the stirring speed increased to 300 rpm. After a few minutes, the initiator APS (0.5 g, 2.2 mmol) dissolved in 5 g of water was added to initiate the polymerization. The temperature was maintained at 75 °C for 24 h to ensure total decomposition of the initiator. The final latex was filtered through a fine nylon mesh to remove any trace of coagulum or dust. A similar latex based on PMMA was also synthesized by substituting the St for the same weight of MMA in the above recipe. In both cases the conversion of monomers to seed polymer particle was quantitative, as judged by dry weight analysis using a moisture analyzer balance (Sartorius MA 35, Germany). Analytical characterization of these particles is presented in the Results and Discussion section.

After completion of the synthesis, the particles were ultrafiltered through a membrane (Millipore Biomax PB) with a molecular cutoff of 300 kDa in a home-built ultrafiltration cell to remove low molecular weight species, e.g., oligomers, emulsifier, undecomposed initiator, or electrolyte from the latex particles. The latex was repeatedly rediluted with distilled deionized water and the ultrafiltration continued under air pressure (5 bar) until the conductivity of the filtrate was constant and low (~10 μS). The colloid was then concentrated to a paste on the ultrafiltration membrane and removed to a flask, and the solid content of the paste was measured using a moisture analyzer balance before being used in the next step.

Derivatization of the Seed Particles. To form the surface iniferter, DEDTC was coupled to the core particles by adding 0.833 g of DEDTC dissolved in 20 mL of tetrahydrofuran (THF) to a suspension of 2.5 g of solid seed particles in 70 mL of THF. The resulting suspension was then transferred to a glass reactor equipped with a reflux condenser and heated at 60 °C under dark conditions with gentle stirring for about 24 h. After derivatization was complete, an excess amount of methanol was added. This caused aggregation allowing the particles to be centrifuged and the solvent to be removed. The particles were washed again with methanol. The final solvent was removed, and the particles were dried to a constant weight at room temperature. The reaction was verified using FTIR and elemental analysis measurements (see Results and Discussion). The dried particles were stored in a sealed tube at room temperature in the dark until used.

Synthesis of Core−Shell Nanoparticles. Polymer layers were grafted from the initiator nanoparticle seeds by addition of the required monomers, EGDMA cross-linker (if necessary), and solvents (toluene, chloroform, dimethylformamide (DMF) or a mixture of toluene and DMF), purging with argon, and then sealing and placing under a UV lamp (high-intensity UV inspection lamp from UVP Ltd., Cambridge, UK) for 11 h. A tube with a water jacket maintained at 25 °C was used for such reactions to prevent heating from the UV lamp, and a small magnetic stir bar was used to provide mixing. A typical experiment used about 50 mg of seed, 40 mg of monomer, 150 mg of cross-linker (if required), and 4 mL of solvent. The resulting polymers were washed by repeated centrifugation and resuspension with methanol, to remove ungrafted monomers or cross-linker, and then dried prior to analysis by a variety of methods. The complex multilayer particles were synthesized by the aforementioned method, where the third stage monomer was used at a 1:0.80 (seed:monomer) weight ratio. Toluene and DMF were used as resuspension medium for the first and second layer synthesis, respectively. The particles generated were characterized by FTIR, elemental analysis, TEM, and dynamic light scattering (DLS) (see Results and Discussion section).

Dynamic Light Scattering (DLS). Measurements were conducted using a Malvern Zetasizer Nano ZS instrument, which allowed calculation of the intensity-average diameter of the latex particles, D_i, via the Stokes−Einstein equation. Particles suspended in an appropriate organic solvent were analyzed using glass cuvettes, and the results were averaged over three consecutive runs. Samples were passed through 0.45 μm syringe filters to remove any large contaminant particles prior to analysis.

Transmission Electron Microscopy (TEM). TEM was used to investigate the shapes and morphologies of the polymer particles. Normally samples were prepared by drying a drop of a dilute (~0.5 wt %) latex dispersion onto a carbon-coated copper grid and analyzed using a JEOL EX2000 electron microscope operating at 120 kV. During morphological investigations we found that the application of staining techniques is absolutely necessary, particularly for the core−shell structures in the size range below or just above 100 nm. Without staining, nanoparticles showed low contrast and experienced a loss of structure or fused together under the electron beam. In our study both negative and positive staining have been applied for morphological characterization. In the case of negative staining, 1 drop of latex was mixed with 1 mL of 2% aqueous or organic (depending upon the solvent used for particle synthesis) PTA solution, and the mixture was allowed to stand for 1 h. Then a drop of diluted dispersion was placed on a carbon-coated Formvar copper grid. A small piece of filter paper was used to remove as much of the drop as possible, leaving a very thin layer of the latex on the grid. For single staining this copper grid was used directly for TEM investigation, but for multiple staining, the PTA-stained sample on a copper grid was placed in a closed Petri dish and reacted with RuO_4 vapor for about 30 min. The RuO_4 vapor was used as a positive stain, and it was prepared by mixing 0.2 g of ruthenium trichloride hydrate with 10 mL of 5.25% aqueous sodium hypochlorite. The fresh mixture is dark red and should be used immediately since it deteriorates (turning black) within a few hours.

Fourier Transform Infrared Spectroscopy (FT-IR). FT-IR measurements were carried out on small dried polymer samples using a single-pass diamond ATR attachment in a Perkin-Elmer BX FTIR instrument. The spectral resolution was set at 4 cm^{-1}, and typically 32 scans were averaged per spectrum.

Aqueous Zeta Potential Titration Studies. Measurements were conducted using a Malvern Zetasizer NanoZS instrument equipped with an autotitrator (MPT-2 multipurpose titrator, Malvern Instruments). The zeta potential, ξ, of selected copolymer latexes was determined as a function of pH in the presence of 1 mM NaCl, using NaOH or HCl to adjust the pH as required.

Elemental Microanalysis. CNS microanalyses were determined in-house using a Carlo Erba 1108 elemental analyzer. The technique used is based on dynamic flash combustion in a 1000 °C furnace with high-purity oxygen. The resultant gas plug is separated in a GC column with components C, N, and S detected as CO_2, NO_2, and SO_2, respectively, with a thermal conductivity detector. About 10 mg of sample was placed into a tin foil boat for each analysis.

Results and Discussion

Core−shell polymeric nanoparticles were synthesized by the described SIP method using a wide range of functional second stage monomers. Based on St and MMA, two sets of cross-linked core particles were prepared containing benzyl chloride functionalities. The particles were washed, and then the DEDTC was coupled to the particle surface. In contrast to the aqueous conditions used by Kawaguchi,[68] this step was carried out in THF to avoid coagulation of the colloidal seeds as the particle surfaces become more hydrophobic during derivatization. The presence of benzyl chloride functionalities and DEDTC coupling to the core particles were checked by FTIR spectroscopy. FTIR spectra in Figure 2 demonstrate successful synthesis of derivatized PS core particles. Comparison of the spectra for the final iniferter particles and the PS-VBCl precursor particles in Figure 2 revealed that the intensity of a characteristic C−Cl peak at 1264 cm^{-1}, initially present from the vinylbenzyl chloride, was significantly increased after derivatization with DEDTC due to the introduction of a C−N stretch band that overlaps any residual C−Cl signal. New peaks appeared at 1209, 1406, 1512 (shoulder), and 990 cm^{-1} (shoulder). All of these peaks can be clearly seen in the spectrum of benzyl diethyldithiocarbamate, a low molecular weight analogue of the surface bound iniferter structure (synthesized in-house from benzyl chloride and sodium diethyldithiocarbamate). These changes, together with elemental analysis data showing the appearance of much greater levels of S and N; see later discussion), provide strong evidence for the derivatization of the PS core particles.

The increase in particle size caused by each new layer grafted to the particle surface was followed by dynamic light scattering,

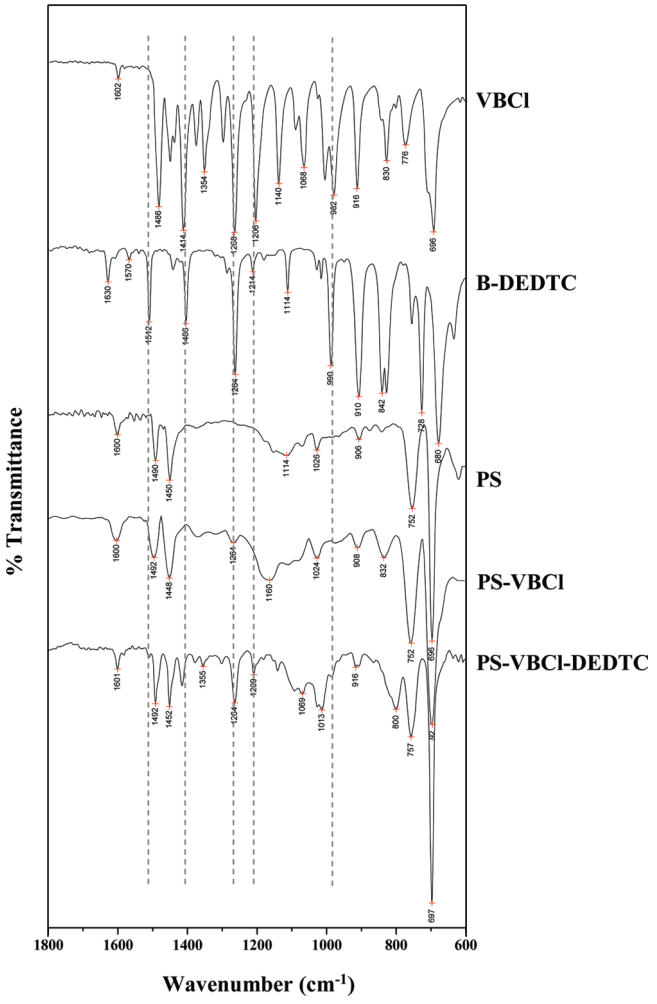

Figure 2. FT-IR spectrum of the iniferter-derivatized PS seed particles. Spectra for relevant precursor particles, monomers, and benzyl diethyldithiocarbamate, a low MW analogue of the surface iniferter, are shown for comparison.

confirming the growth of new layers over the pre-existing ones (Figure 3). The nanoparticles had a relatively narrow size distribution. The size increased with the addition of new layers. No new particle nucleation was observed, consistent with an effective SIP process, where only radicals bound to the particle surface are capable of initiating polymerization. The fact that the particle size distribution did not increase markedly as new layers were added also suggests a rather uniform growth of the polymer layers, consistent with a well-controlled living-radical process. The grafted polymer layer thickness was very uniform at about 5 nm, despite using a variety of different monomers. The size distribution data after a second stage polymerization with cross-linker (Figure 3, right side) also confirms the monodispersity of the copolymer latexes and demonstrates that no gelation was evident, despite the relatively high levels of cross-linker used and the high seed and monomer loadings in the system (typically 1−2 wt % seed and up to 5 wt % monomers). When the cross-linker was included, the shell thickness was approximately double that obtained for the linear polymer shells, but again there was relatively little difference between the different functional monomers tested.

The incorporation of the indicated monomers into the iniferter seed particles after UV polymerization was confirmed by FT-IR analysis (see Figure 4). After the second stage polymerization the main characteristic peaks appearing in addition to the PS* core for the different monomers incorporated are given below:

PS*: peaks at 2923 and 3025 cm^{-1} correspond to aliphatic (backbone) and aromatic-C−H stretching. The peaks at 697 and 1601 cm^{-1} appear for monosubstituted benzene and C=C stretching, respectively.

PS*-PMMA: peaks at 1729 and 1146 cm^{-1} correspond to C=O and C−O stretching, respectively, from the newly introduced ester group of PMMA.

PS*−PNIPAM: peaks at 1644 and 1536 cm^{-1} correspond to C=O and C−N stretching of the side-chain amide.

PS*−PHEMA: peaks at 1716 and 3700−3100 cm^{-1} correspond to C=O (of the ester) and terminal O−H stretching from the side chain.

PS*−PMAA: peak at 1700 cm^{-1} corresponds to C=O of the carboxylic acid. Peaks at 1168 and 3100−3700 cm^{-1} represent C−OH and O−H...O stretching, respectively.

PS*-PDEAMA: peaks at 1698 and 1228 cm^{-1} corresponds to C=O and C−N stretching, respectively.

Thus, in each case, new peaks characteristic of the incorporation of the expected monomer were clearly visible, confirming that a second-stage polymerization had occurred. The fact that these signals were recorded after extensive washing of the particles confirms that the new monomers were polymerized into the structure, and not just absorbed, causing swelling of the particle. It is interesting to contrast the polymer layer thickness for poly(NIPAM) generated under these conditions with the very much greater layer thicknesses generated with shorter irradiation times under aqueous conditions in Kawaguchi's work.[68,69] Presumably, this largely reflects the very much higher polymerization rate for this monomer in water although there may also have been some difference in UV irradiation intensity. Under the conditions used in this work, NIPAM showed very similar behavior to a range of other monomers and produced thin (5−10 nm) films, suggesting a much slower rate of polymerization and consequently much better control for generating thin layers. The iniferter surface density on our particles is also much higher (see later discussion) than the polymer graft density they reported, suggesting that our shells have a high density of short chains, compared with the long, isolated "hairs" produced on their (much larger) particles under aqueous conditions. The high iniferter density and large surface area in our nanoparticle system would tend to increase the concentration of dithiocarbamate radicals present at any time, which may also contribute to the observed effect, through more frequent termination and reinititation. This would be analogous to the use of additional tetraethylthiuram disulfide in the solvent phase to control surface grafting reactions.[76]

Taken together, the FTIR and particle size data confirm that new monomers have been incorporated into the polymer particles, but it does not explicitly identify the location of this incorporation. It has been assumed that polymerization takes place at the surface, since the core is cross-linked, precluding polymer reorganization and phase separation often seen in heterophase polymerizations,[77] but in order to confirm this, it is necessary to investigate the particle morphology by TEM. The morphology characterization of nanosized composite polymer particles is not easy as it requires the identification of morphological features with dimensions well below 100 nm in soft, low electron density materials that provide little contrast in TEM. Such particles can easily suffer a loss of structure or fuse together under the electron beam. During the morphological investigation we found that the application of staining techniques is absolutely necessary, particularly for composite particles with core−shell structures in the size range below or just above 100 nm. By applying suitable staining techniques, it was possible to obtain informative images. A TEM image of a PS seed is shown in Figure 5a and confirms the general observation of the DLS measurements, i.e., that the particles are fairly monodisperse.

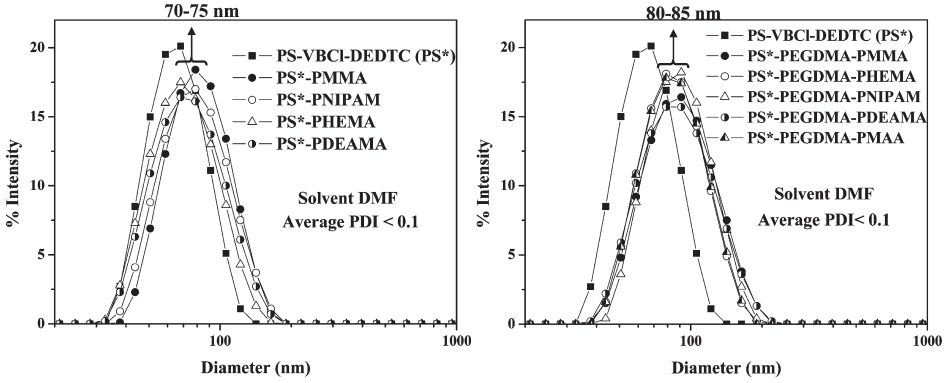

Figure 3. Particle size distributions measured by dynamic light scattering showing the increase in particle size after the second stage polymerization onto the core particle, using a variety of different monomers with (right side) and without (left side) cross-linker. DMF was used as second stage polymerization solvent and also the solvent in which the size measurements were made.

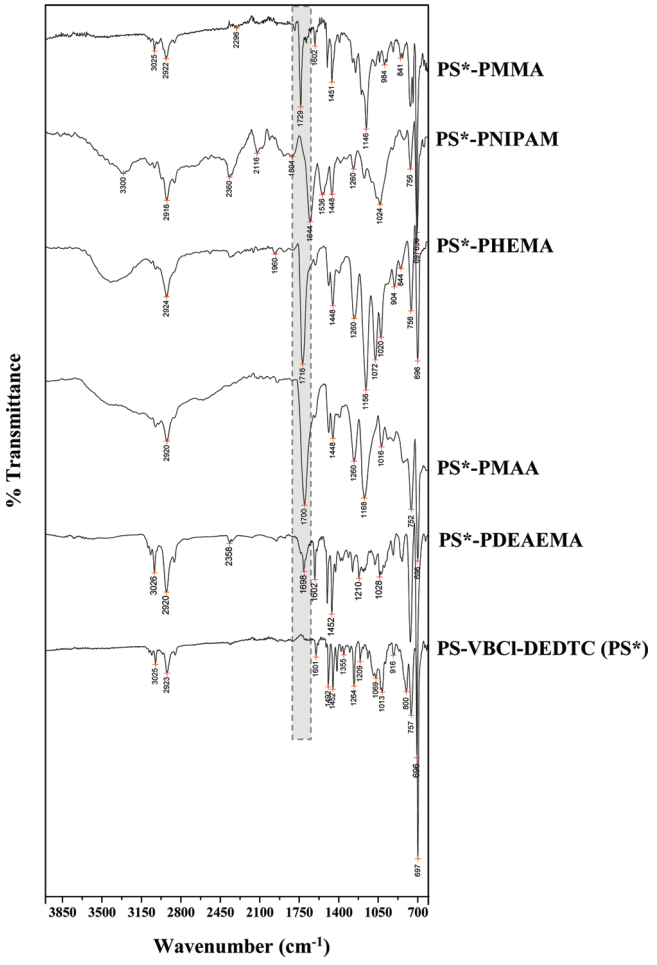

Figure 4. FT-IR spectra showing the evidence of polymer grafting after the second stage polymerization. A PS-VBCl-DEDTC (PS*) reference polymer is also included for comparison.

This particular seed has a number-average diameter of 55 nm when imaged under vacuum by TEM. After the second stage polymerization, a core−shell structure is clearly formed as expected (Figure 5b). The number-average size increased from 55 to 80 nm, where PS forms the core region which appears dark and PMMA forms the shell region which appears bright. The core−shell structure is also observable in case of polymeric nanoparticles where HEMA and EGDMA are used as second stage monomer and cross-linker respectively (see Figure 5c). Again PEGDMA−PHEMA forms the shell region which appears bright, and the number-average diameter increased from 55 to 90 nm. The thicker shell is clearly visible in the image, when compared with the much thinner bright shell rings in Figure 5b. This is consistent with the DLS measurement of the solvated particles shown in Figure 3. It is clear that the covalent surface grafting process, coupled with the use of a cross-linked core, prevents any polymer chain reorganization and phase separation occurring; hence, clear core−shell structures are obtained, and there is no tendency to generate alternative morphologies, as sometimes produced in other types of heterophase polymerizations.[77]

We have also synthesized core−shell nanoparticles by using PMMA−VBCl−DEDTC (PMMA*) as core and styrene as shell monomer to verify the versatility of the approach (Figure 6). After the second stage polymerization the intensity average diameter of the core particles increased from 58 to 68 nm, showing the formation of the PS shell layer on the PMMA core particle. Figure 6 also confirms that the particle size distribution is very narrow and the average particle polydispersity index (PDI) is less than 0.1, indicating that the particles were near monodisperse.

FTIR analysis (Figure 7) also revealed the successful grafting of the second stage polymer PS onto the PMMA core particles. The much more prominent peak at 700 cm^{-1} is characteristic of the monosubstituted bezene ring, which has been greatly enhanced by the incorporation of the PS layer. A peak also appears at 1606 cm^{-1} for C=C stretching of PS.

Aqueous zeta potential titration studies of two selected second-stage copolymer latexes and a reference latex are shown in Figure 8. For each ionic monomer, the expected solution behavior was observed. Thus, the cationic DEAEMA second stage monomer led to positive zeta potentials at low pH, whereas the anionic MAA second stage monomer gave significantly more negative zeta potentials than that of the reference polymer at neutral pH. Although it is difficult to estimate the pK_a values accurately from these curves (due to some underlying behavior from residual sulfate groups from the initial seed polymerization), it is evident that the zeta potential titration curves mirror the expected ionization curves for polymers containing ionic monomers with pK_a values similar to MAA and DEAEMA. Thus, it appears that the surface functionalization of PS-based copolymer latexes can be easily modified by copolymerization with various ionic monomers, which may be important for applications where surface charge manipulation is essential for function or to manipulate colloid stability.

By applying the surface-initiated living radical mechanism sequentially, we have also synthesized complex multilayer nanoparticles. Such sequential layer grafting onto the polymeric nanoparticles was demonstrated by growing two polymeric layers

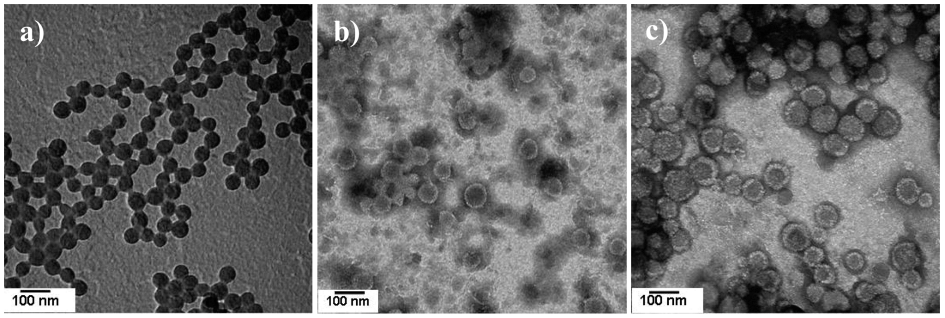

Figure 5. TEM images of polymer nanoparticles: (a) PS-VBCl seed stained with phosphotungstic acid (PTA); (b) PS*−PMMA and (c) PS*−PEGDMA−PHEMA core−shell nanoparticles prepared using toluene and chloroform as second stage polymerization solvent, respectively. For TEM imaging both core−shell nanoparticles are stained with PTA/RuO_4.

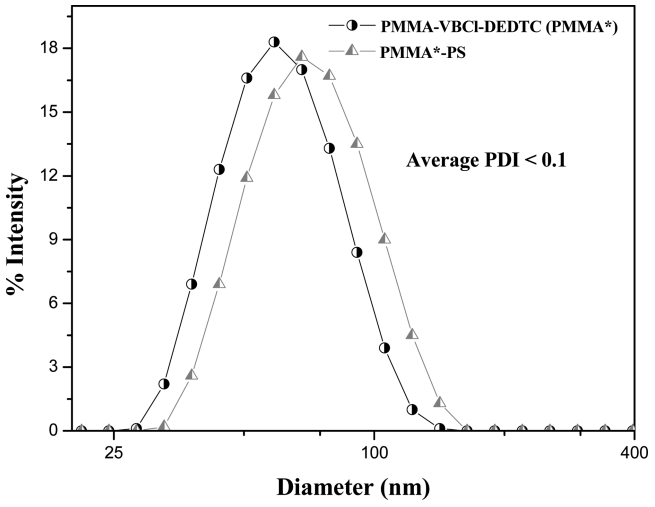

Figure 6. Particle size distributions measured by dynamic light scattering showing the increase in particle size after the second stage polymerization of PS onto the PMMA core particle. DMF was used as the second stage polymerization solvent.

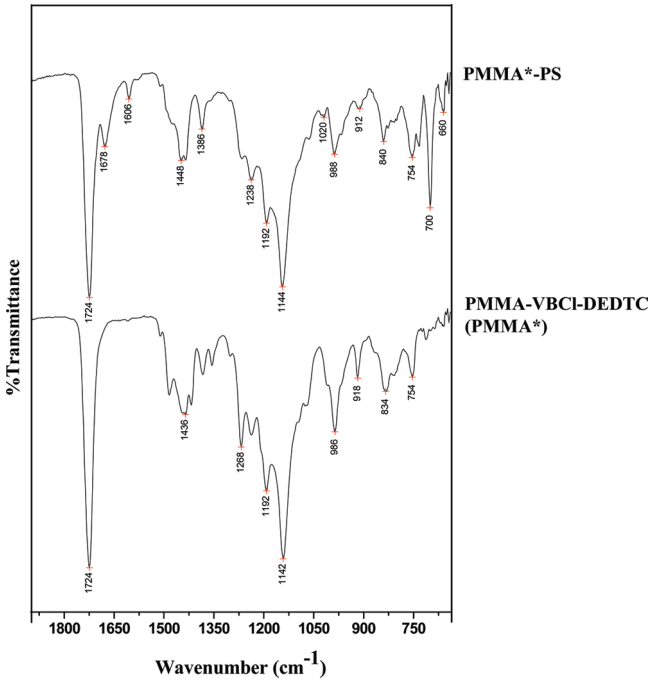

Figure 7. FT-IR spectra showing evidence of PS grafting after the second stage polymerization.

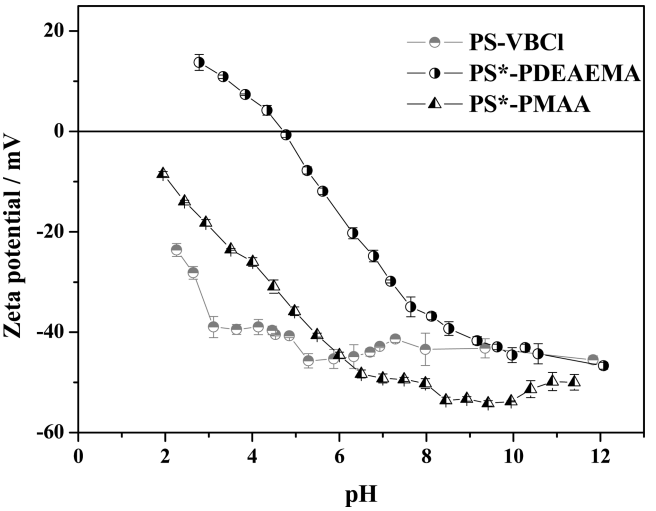

Figure 8. Aqueous zeta potential titration curves obtained for copolymer nanoparticles prepared by surface-initiated polymerization. A PS-VBCl seed latex is also included as a reference.

over a monodisperse seed of PS−VBCl−DEDTC (PS*). The particles were synthesized for the purpose of demonstration only, and monomers were chosen for easy identification (see Figure 9). This particular particle thus has no specific function but was prepared to demonstrate the control and flexibility of the approach.

DLS data supports the increase in particle size caused by sequential layer formation. The size distribution data in Figure 9a shows the significant increase in particle size. The intensity average size of the seed particles increased from 64 to 110 nm after the first layer formation, and it further increased to 140 nm after the second layer formation (note that DMF was used as measurement solvent). The mean particle diameters were always higher than the number-average diameters measured from TEM images (data not shown). This is easily understandable, since light scattering provides an intensity-average diameter, which is always influenced by the solvation of the polymer layer, making an additional contribution to the overall diameter of the solvated particles, whereas this solvated layer is expected to dry down to a much reduced thickness under the ultrahigh-vacuum conditions used for electron microscopy. The DLS data also show a relatively narrow size distribution without any secondary nucleation, indicating an effective SIP process.

The formation of PS*−PMMA−PMAA multilayer polymeric nanoparticles was also analyzed by FT-IR spectroscopy (see Figure 9b). This confirmed the grafting of the PMMA first shell onto the PS* core particles by the appearance of two important peaks at 1728 and 1146 cm^{-1} for C═O and C−O stretching, respectively. The formation of the second PMAA shell was

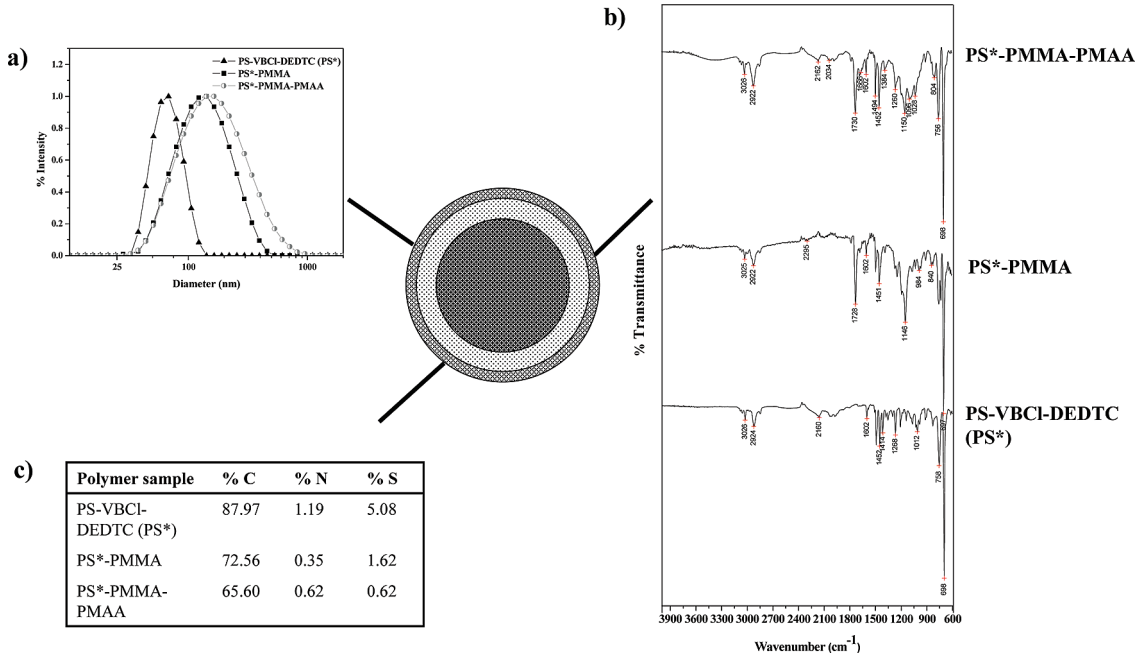

c)

Polymer sample	% C	% N	% S
PS-VBCl-DEDTC (PS*)	87.97	1.19	5.08
PS*-PMMA	72.56	0.35	1.62
PS*-PMMA-PMAA	65.60	0.62	0.62

Figure 9. Sequential layer grafting onto a PS−VBCl−DEDTC (PS*) nanoparticle. (a) Particle size distributions measured by dynamic light scattering shows the increase in particle size after addition of new layers onto the core particle. (b) FT-IR spectra show the evidence of polymer grafting for each layer. (c) Elemental analysis shows the retention of sulfur content after addition of the second layer (taking into account the overall mass increase due to the new layer added).

confirmed by the presence of acidic functionality. The broad carboxylic acid absorbance is observable between 3200 and 3700 cm^{-1} adjacent to the PS C−H stretching peaks from 2750 to 3200 cm^{-1}. The OH...O in-plane deformation, coupled to the C−O stretching vibration, is easy to observe as a band with medium intensity, appearing at 1384 cm^{-1}. The peak at 1146 cm^{-1} which appears for the C−O stretching band of PMMA polymer also shifted slightly toward higher wavenumber (1150 cm^{-1}) because of the C−OH stretching band that appears for the PMAA second shell.

Finally, it has been confirmed by elemental analysis that the formation of multilayer polymeric nanoparticles followed the living radical mechanism. Sulfur analysis (see Figure 9c) shows that there is almost complete retention of the iniferter (after accounting for the volume increase; see Supporting Information for calculations and assumptions made) at the particle surface after the first shell has been formed, confirming that the dithiocarbamate acts by a living radical mechanism and that almost no chain termination or chain transfer occurs other than to reform the iniferter; i.e., it behaves in a model living radical manner. The iniferter can thus be used to form additional polymer layers over the top of the first shell, as demonstrated by us in a preliminary report on the use of this approach for molecular imprinting,[64] though it should be noted that as the particle size increases, the iniferter groups will become somewhat more isolated, so it is not clear how complete subsequent layers may be and how this might affect particle properties. The surface iniferter loading of the core particles was estimated to be ~4.4 per nm^2 from elemental analysis coupled with geometric calculations for spheres of density 1 g cm^{-3}. This is quite similar to the ATRP initiator density reported by Jayachandran et al.[74] for a much larger polystyrene latex. The high iniferter density suggests that the chain grafting could be rather dense, and even after shell growth there would still be above 1 iniferter per nm^2 for further particle elaboration. The high degree of iniferter retention, despite the close proximity of growing chains, indicates that there is minimal chain end recombination. This suggests that the vast majority of chain ends are dormant at any point in time and is consistent with the slow shell growth rate observed in this work. Retention of iniferter also appears to be sensitive to the monomers and solvents used. While the MMA/toluene pair used for the first layer behaved in a model manner, the MAA/DMF pair used for the second shell showed only 55% iniferter retention. The increase in the elemental N content suggests that the main reason for loss may be due to chain transfer to solvent, or even UV photoreduction of DMF to generate radicals,[78] but this has not been investigated in detail. Whatever the mechanism, it did not lead to system gelation in our studies (even when cross-linker is present), suggesting that propagation of solution-phase radicals is minimal.

Conclusion

Stable polymeric core−shell nanoparticles have been readily prepared via surface-initiated polymerization. This process makes it possible to produce fairly monodisperse core−shell nanoparticles (below 100 nm) with good control over the size distribution. The composition of the polymeric shell layer has been confirmed by FT-IR analysis and the core−shell structure of the nanoparticle by TEM. It has also been established that a wide range of monomers and solvents can be used to prepare polymeric core−shell nanoparticles using this approach. Finally, it is possible to graft sequential layers with diverse properties on the same particles by this living radical SIP method, demonstrating the flexibility and utility of the approach. Because of the non-aqueous nature of the system, it should also be possible to introduce a variety of water-labile or highly water-soluble functionalities, which would be difficult or impossible to incorporate into conventional aqueous core−shell synthesis methods. We thus anticipate that this generic approach to core−shell particle synthesis by SIP will be useful in a diverse range of applications in the future.

Acknowledgment. The authors thank the BBSRC (Grant BB/D011949/1) for funding this work. The assistance of Dr. Colin McDonald with the TEM and Mr. Graham Chilvers with the elemental analysis is also gratefully acknowledged.

Supporting Information Available: Recipes and conditions of polymer grafting onto core nanoparticles and calculation of the retention of iniferter after sequential layer grafting onto a PS−VBCl−DEDTC (PS*) core nanoparticle. This material is available free of charge via the Internet at http://pubs.acs.org.

References and Notes

(1) Atkinson, W. I. *Nanocosm: Nanotechnology and the Big Changes Coming from the Inconceivably Small*. AMACOM: New York, 2005.
(2) Kirsch, S.; Landfester, K.; Shaffer, O.; El-Aasser, M. S. *Acta Polym*. **1999**, *50*, 347–362.
(3) Devon, M. J.; Gardon, J. L.; Roberts, G.; Rudin, A. *J. Appl. Polym. Sci*. **1990**, *39*, 2119–2128.
(4) Dimonie, V.; Elaasser, M. S.; Klein, A.; Vanderhoff, J. W. *J. Polym. Sci., Part A: Polym. Chem*. **1984**, *22* (9), 2197–2215.
(5) Pusch, J.; van Herk, A. M. *Macromolecules* **2005**, *38* (16), 6909–6914.
(6) Grancio, M. R.; Williams, D. J. *J. Polym. Sci., Part A-1: Polym. Chem*. **1970**, *8* (9), 2617–&.
(7) Jonsson, J. E.; Hassander, H.; Tornell, B. *Macromolecules* **1994**, *27* (7), 1932–1937.
(8) Durant, Y. G.; Sundberg, E. J.; Sundberg, D. C. *Macromolecules* **1997**, *30* (4), 1028–1032.
(9) Lee, C. F.; Young, T. H.; Huang, Y. H.; Chiu, W. Y. *Polymer* **2000**, *41* (24), 8565–8571.
(10) Okubo, M.; Ahmad, H. *J. Polym. Sci., Part A: Polym. Chem*. **1996**, *34* (15), 3147–3153.
(11) Ahmad, H.; Ali, A. M. I.; Miah, M. A. J. *J. Polym. Mater*. **2001**, *18* (3), 287–292.
(12) Okubo, M.; Izumi, J. *Colloids Surf., A* **1999**, *160* (3), 321–321.
(13) Okubo, M.; Izumi, J. *Colloids Surf., A* **1999**, *153* (1−3), 297–304.
(14) Okubo, M.; Izumi, J.; Hosotani, T.; Yamashita, T. *Colloid Polym. Sci*. **1997**, *275* (8), 797–801.
(15) Okubo, M.; Izumi, J.; Takekoh, R. *Colloid Polym. Sci*. **1999**, *277* (9), 875–880.
(16) Okubo, M.; Minami, H.; Fujii, S.; Mukai, T. *Colloid Polym. Sci*. **1999**, *277* (9), 895–899.
(17) Takahashi, K.; Nagai, K. *Polymer* **1996**, *37* (7), 1257–1266.
(18) Bucsi, A.; Forcada, J.; Gibanel, S.; Heroguez, V.; Fontanille, M.; Gnanou, Y. *Macromolecules* **1998**, *31* (7), 2087–2097.
(19) Nagai, K. *Trends Polym. Sci*. **1996**, *4* (4), 122–127.
(20) Hirose, M.; Zhou, J. H.; Nagai, K. *Prog. Org. Coat*. **2000**, *38* (1), 27–34.
(21) Furusawa, K.; Anzai, C. *Colloid Polym. Sci*. **1987**, *265* (10), 882–888.
(22) Okubo, M.; He, Y.; Ichikawa, K. *Colloid Polym. Sci*. **1991**, *269* (2), 125–130.
(23) Okubo, M.; Ichikawa, K.; Tsujihiro, M.; He, Y. *Colloid Polym. Sci*. **1990**, *268* (9), 791–796.
(24) Okubo, M.; Lu, Y. *Colloid Polym. Sci*. **1996**, *274* (11), 1020–1024.
(25) Okubo, M.; Miyachi, N.; Lu, Y. *Colloid Polym. Sci*. **1994**, *272* (3), 270–275.
(26) Okubo, M.; Lu, Y.; Wang, Z. *Colloid Polym. Sci*. **1998**, *276* (9), 833–837.
(27) Okubo, M.; Lu, Y.; Wang, Z. *Colloid Polym. Sci*. **1999**, *277* (1), 77–82.
(28) Okubo, M.; Lu, Y. *Colloids Surf., A* **1996**, *109*, 49–53.
(29) Fleming, M. S.; Mandal, T. K.; Walt, D. R. *Chem. Mater*. **2001**, *13* (6), 2210–2216.
(30) Schneider, G.; Decher, G. *Nano Lett*. **2004**, *4* (10), 1833–1839.
(31) Caruso, F.; Caruso, R. A.; Mohwald, H. *Chem. Mater*. **1999**, *11* (11), 3309–3314.
(32) Caruso, F.; Spasova, M.; Susha, A.; Giersig, M.; Caruso, R. A. *Chem. Mater*. **2001**, *13* (1), 109–116.
(33) Caruso, R. A.; Susha, A.; Caruso, F. *Chem. Mater*. **2001**, *13* (2), 400–409.
(34) O'Reilly, R. K.; Joralemon, M. J.; Hawker, C. J.; Wooley, K. L. *J. Polym. Sci., Part A: Polym. Chem*. **2006**, *44* (17), 5203–5217.
(35) Quirk, R. P.; Mathers, R. T.; Cregger, T.; Foster, M. D. *Macromolecules* **2002**, *35* (27), 9964–9974.
(36) Zhao, B.; Brittain, W. J. *Macromolecules* **2000**, *33* (2), 342–348.
(37) Kong, X. X.; Kawai, T.; Abe, J.; Iyoda, T. *Macromolecules* **2001**, *34* (6), 1837–1844.
(38) Husseman, M.; Malmstrom, E. E.; McNamara, M.; Mate, M.; Mecerreyes, D.; Benoit, D. G.; Hedrick, J. L.; Mansky, P.; Huang, E.; Russell, T. P.; Hawker, C. J. *Macromolecules* **1999**, *32* (5), 1424–1431.
(39) Prucker, O.; Ruhe, J. *Macromolecules* **1998**, *31* (3), 602–613.
(40) Nakayama, Y.; Matsuda, T. *Macromolecules* **1996**, *29* (27), 8622–8630.
(41) Nakayama, Y.; Matsuda, T. *Langmuir* **1999**, *15* (17), 5560–5566.
(42) Zhao, B.; Brittain, W. J. *Prog. Polym. Sci*. **2000**, *25* (5), 677–710.
(43) Hadjichristidis, N.; Pitsikalis, M.; Iatrou, H.; Pispas, S. *Macromol. Rapid Commun*. **2003**, *24* (17), 979–1013.
(44) Edmondson, S.; Osborne, V. L.; Huck, W. T. S. *Chem. Soc. Rev*. **2004**, *33* (1), 14–22.
(45) Santer, S.; Ruhe, J. *Polymer* **2004**, *45* (25), 8279–8297.
(46) Boyes, S. G.; Granville, A. M.; Baum, M.; Akgun, B.; Mirous, B. K.; Brittain, W. J. *Surf. Sci*. **2004**, *570* (1−2), 1–12.
(47) Matsuda, T. *Adv. Polym. Sci*. **2006**, *197*, 67–106.
(48) Zdyrko, B.; Hoy, O.; Kinnan, M. K.; Chumanov, G.; Luzinov, I. *Soft Matter* **2008**, *4* (11), 2213–2219.
(49) Deng, J. P.; Wang, L. F.; Liu, L. Y.; Yang, W. T. *Prog. Polym. Sci*. **2009**, *34* (2), 156–193.
(50) Advincula, R. C. *J. Dispersion Sci. Technol*. **2003**, *24* (3−4), 343–361.
(51) Advincula, R. *Adv. Polym. Sci*. **2006**, *197*, 107–136.
(52) Park, J. T.; Koh, J. H.; Koh, J. K.; Kim, J. H. *Appl. Surf. Sci*. **2009**, *255* (6), 3739–3744.
(53) Lee, H. Y.; Rwei, S. P.; Wang, L.; Chen, P. H. *Mater. Chem. Phys*. **2008**, *112* (3), 805–809.
(54) Reddy, K. R.; Lee, K. P.; Kim, J. Y.; Lee, Y. *J. Nanosci. Nanotechnol*. **2008**, *8* (11), 5632–5639.
(55) Berger, S.; Synytska, A.; Ionov, L.; Eichhorn, K. J.; Stamm, M. *Macromolecules* **2008**, *41* (24), 9669–9676.
(56) Dong, H. C.; Zhu, M. Z.; Yoon, J. A.; Gao, H. F.; Jin, R. C.; Matyjaszewski, K. *J. Am. Chem. Soc*. **2008**, *130* (39), 12852–+.
(57) Chen, F. H.; Gao, Q.; Hong, G. Y.; Ni, J. Z. *J. Magn. Magn. Mater*. **2008**, *320* (13), 1921–1927.
(58) Zirbs, R.; Binder, W.; Gahleitner, M.; Machl, D. In *"Grafting From" - Living Cationic Polymerization of Poly(isobutylene) from Silica-Nanoparticle Surfaces*; 3rd International Symposium on Reactive Polymers in Inhomogeneous Systems, in Melts and at Interfaces, Dresden, Germany, Sep 23−26, 2007; Wiley-VCH: Dresden, 2007; pp 93−96.
(59) Lei, Z. L.; Bi, S. X. *Mater. Lett*. **2007**, *61* (16), 3531–3534.
(60) Sun, Y. B.; Ding, X. B.; Zheng, Z. H.; Cheng, X.; Hu, X. H.; Peng, Y. X. *Eur. Polym. J*. **2007**, *43* (3), 762–772.
(61) Fulghum, T. M.; Patton, D. L.; Advincula, R. C. *Langmuir* **2006**, *22* (20), 8397–8402.
(62) Radhakrishnan, B.; Ranjan, R.; Brittain, W. J. *Soft Matter* **2006**, *2* (5), 386–396.
(63) Joubert, M.; Delaite, C.; Lami, E. B.; Dumas, P. *New J. Chem*. **2005**, *29* (12), 1601–1609.
(64) Bao, H.; Chumanov, G.; Czerw, R.; Carroll, D. L.; Foulger, S. H. *Colloid Polym. Sci*. **2005**, *283* (6), 653–661.
(65) Schmidt, A. M. *Macromol. Rapid Commun*. **2005**, *26* (2), 93–97.
(66) Blomberg, S.; Ostberg, S.; Harth, E.; Bosman, A. W.; Van Horn, B.; Hawker, C. J. *J. Polym. Sci., Part A: Polym. Chem*. **2002**, *40* (9), 1309–1320.
(67) Jordan, R.; West, N.; Ulman, A.; Chou, Y. M.; Nuyken, O. *Macromolecules* **2001**, *34* (6), 1606–1611.
(68) Kawaguchi, H.; Isono, Y.; Tsuji, S. *Macromol. Symp*. **2002**, *179*, 75–87.
(69) Tsuji, S.; Kawaguchi, H. *Langmuir* **2004**, *20* (6), 2449–2455.
(70) Tsuji, S.; Kawaguchi, H. *Macromolecules* **2006**, *39* (13), 4338–4344.
(71) Otsu, T.; Yoshida, M. *Makromol. Chem., Rapid Commun*. **1982**, *3* (2), 127–132.
(72) Otsu, T. *J. Polym. Sci., Part A: Polym. Chem*. **2000**, *38* (12), 2121–2136.
(73) Guerrini, M. M.; Charleux, B.; Vairon, J. P. *Macromol. Rapid Commun*. **2000**, *21* (10), 669–674.
(74) Jayachandran, K. N.; Takacs-Cox, A.; Brooks, D. E. *Macromolecules* **2002**, *35* (11), 4247–4257.
(75) Pérez-Moral, N.; Mayes, A. G. *Macromol. Rapid Commun*. **2007**, *28* (22), 2170–2175.
(76) Byrne, M. E.; Oral, E.; Hilt, J. Z.; Peppas, N. A. *Polym. Adv. Technol*. **2002**, *13* (10−12), 798–816.
(77) Sundberg, D. C.; Durant, Y. G. *Polym. React. Eng*. **2003**, *11* (3), 379–432.
(78) Yang, P.; Deng, J. Y.; Yang, W. T. *Macromol. Chem. Phys*. **2004**, *205* (8), 1096–1102.